

# Intriguing electron correlation effects in the photoionization of metallic quantum dot nanorings

Ioan Bâldea, Lorenz S. Cederbaum, and Jochen Schimmer

Theoretische Chemie, Physikalisch-Chemisches Institut, Universität Heidelberg,

Im Neuenheimer Feld 229, D-69120 Heidelberg, Germany

(Dated: February 20, 2024)

## Abstract

We report detailed results on ionization in metallic quantum dot (QD) nanorings described by the extended Hubbard model at half filling obtained by exact numerical diagonalization. In spite of very strong electron correlations, the ionization spectra are astonishingly scarce. We attribute this scarcity to a hidden quasi-symmetry, generalizing thereby similar results on optical absorption recently reported [I. Bâldea and L. S. Cederbaum, Phys. Rev. B 75, 125323 (2007); 77, 165339 (2008)]. Numerical results indicate that this hidden quasi-symmetry of the extended Hubbard model does not evolve into a true (hidden) symmetry but remains a quasi-symmetry in the case of the restricted Hubbard model as well. Based on the observation on the number of significant ionization signals per each spatial symmetry, we claim the existence of a one-to-one map between the relevant ionization signals of the correlated half-filled nanorings and the one-hole and two-hole-one-particle processes possible in the noninteracting case. Similar to the case of optical absorption, numerous avoided crossings (anticrossings) are present in the ionization spectra, which often involve more than two states. The present results demonstrate that ionization could be a useful tool to study electron correlations in metallic QD nanoarrays, providing information that is complementary to optical absorption.

PACS numbers: 79.60.Jv, 78.67.Hc, 71.10.Fd, 71.27.+a

---

Electronic address: ioan@pci.uni-heidelberg.de; Also at National Institute for Lasers, Plasmas, and Radiation Physics, ISS, RO-76900 Bucharest-Magurele, Romania.

## I. INTRODUCTION

Metallic quantum dots (QDs) can be fabricated and assembled in extended regular arrays by means of modern nanotechnologies [1, 2, 3, 4, 5, 6, 7]. The salient feature of such artificial nanostructures is the fact that their electronic properties can be smoothly tuned in wide ranges by factors that can be easily controlled experimentally: dot diameter  $2R$ , interdot spacing  $D$ , and gate potentials. It is this tunability of nanostructures that makes the most important difference from ordinary molecules and solids. In isolated QDs with sizes of a few nanometers, typical for the nanograins of silver prepared by Heath's group [1, 2, 4, 5, 7, 8, 9, 10], the single-electron levels, characteristic for quantum boxes or "artificial" atoms [11], are well separated by energies  $\sim 1$  eV. A small fraction of "valence" electrons, which occupy the highest "atomic" orbitals, becomes delocalized over the whole nanostructure, if the QDs are sufficiently densely packed and the adjacent electronic wave functions overlap.

For nearly touching Ag-QDs ( $d = D - 2R \approx 1$ ), correlations of these delocalized electrons are negligible: the single-particle, molecular-orbital (MO) picture represents a very good approximation [12, 13, 14]. This description progressively worsens for more and more distant QDs, and completely breaks down towards the end of the  $d$ -range of experimental interest ( $d \approx 2$ ). Electron correlations become more and more important beyond  $d \approx 1.4$  [12, 13, 14, 15]. The attractive fact to study such QD nanostructures is that by varying  $d$  one can drive continuously a many-electron system between weak and strong correlation regimes. Obviously, this route from weak to strong correlation regimes is inconceivable in ordinary molecules and solids.

The present paper is devoted to metallic QD nanorings. To our knowledge, rings of metallic QDs have not yet been assembled so far. For this purpose, the use of a mask in the preparation of a two-dimensional nanoarray [1, 2, 4, 5, 7, 8, 9, 10] is conceivable. As shown recently [13, 14], electron correlations in these metallic QD nanorings turned out to possess an intriguing character. In spite of very strong correlations, the optical absorption spectra are astonishingly scarce (almost monochromatic for closed shells [13]) and can be rationalized within a single-particle description. It would be interesting to further investigate to what extent the hidden quasi-symmetry suggested in the context of optical absorption [13, 14] manifests itself in other properties. Along this line, in the present investigation we shall focus

our attention to (photo)ionization, a property for which electron correlations are known to be important [16, 17, 18, 19, 20, 21, 22, 23, 24]. The important role played by electron correlation in the ionization of QD nanorings became evident in the preliminary study of Ref. 12. In this sense, the present work is an extension of the investigation of Ref. 12, where only the lowest energy process was considered. This is the so-called HOMO process, because within the single-particle picture it would correspond to removing an electron from the highest occupied molecular orbital. The fact demonstrated in Ref. 12, that the molecular orbital picture of ionization completely breaks down in QD nanorings even for the HOMO processes is very interesting, because it is contrary to ordinary molecules, where it holds; see Refs. 16, 17, 18, 19, 20, 21. This represents a further motivation for studying ionization in QD nanorings.

To anticipate, the results for ionization we are going to present below fully support the existence of a hidden quasi-symmetry in the strongly correlated metallic QD nanorings described within the extended Hubbard model found in optical absorption [13, 14]. Still, because we cannot present an analytical proof on the existence of a hidden quasi-symmetry, we believe that it is important and beneficial for further investigations to amply document it by detailed exact results obtained by means of extended numerical calculations. Because the numerical study is rather intricate, in Sec. II, where the model of QD nanorings is exposed, we also provide significant details, which were not given in the earlier studies. In the next Sec. III we analyze the electron correlations from a standpoint different from that adopted in Refs. [12, 13, 14], e.g., by considering the quantum entanglement. In Sec. IV, the results on ionization spectra will be presented. We shall examine in detail the cases of nanorings consisting of six and ten QDs separately, in Secs. IV A and IV B, respectively. The two main effects of electron correlations, the avoided crossings and the scarcity of the ionization spectra will be considered in Secs. V and VI, respectively. Conclusions will be presented in the final Sec. VII.

## II. MODEL AND METHOD

To describe the valence electrons of metallic QD nanorings, we shall utilize, similar to a series of previous studies [12, 13, 14, 15, 25], an extended Hubbard (or Pariser-Parr-Pople)

model Hamiltonian

$$H = \sum_{l=1}^N t_{l,l\#} a_{l;1}^\dagger a_{l\#1} + a_{l\#1}^\dagger a_{l;1} + \sum_{l=1}^N \left[ U n_{l;1} n_{l\#} + V n_{l;1} n_{l+1} \right]; \quad (1)$$

where,  $a$  ( $a^\dagger$ ) denote creation (annihilation) operators for electrons,  $n_{l;1} = a_{l;1}^\dagger a_{l;1}$ ,  $n_{l\#} = a_{l\#}^\dagger a_{l\#}$ . The ideal situation assumed in Eq. (1), where the model parameters are site independent, can be considered a reasonable approximation in view of the narrow size distributions ( $\sim 2-5\%$ ) in the arrays of Ag QDs assembled by Heath's group [1, 2, 4, 5, 7]. As previously discussed [12, 13], such a weak disorder does not significantly alter the results obtained by assuming site-independent parameters. Importantly for subsequent considerations, the point symmetry group associated with the model (1) of nanoring is  $D_{Nh}$ .

The model parameter entering Eq. (1) has been analyzed earlier in literature [2, 7, 12, 26, 27, 28, 29] and will be therefore no more repeated here. Importantly, the fact that the interdot separation  $d = D = (2R)$  (measured between QD centers) can be continuously varied in the range  $1.10 \leq d \leq 1.85$  by means of a Langmuir technique allows a wide parameter tuning [1, 2, 4, 5, 7]. For concrete values, see Fig. 1 of Ref. 14. At the ends of the aforementioned  $d$ -range, the ratio of the on-site repulsion  $U$  to the free electron bandwidth  $4t_0$  varies from values  $U = (4t_0) \ll 1$  to  $U = (4t_0) \gg 1$ . Therefore, a crossover from a weakly correlated system to a strongly correlated one by varying  $d$  can be reached.

Ionization is usually described as ejection of an electron from a "molecular" orbital (MO). Therefore, besides electron operators  $a_{l;1}$  for "atomic" orbitals, it is also useful to introduce operators of MOs (or Bloch states),  $c_{k,i} = \frac{1}{\sqrt{N}} \sum_{l=1}^N a_{l;1} \exp(i k l)$ . An ionization signal is characterized by an ionization potential  $\epsilon_{k,i} = \langle H_{k,i} \rangle - \langle H \rangle$  and a spectroscopic factor  $w$

$$w_{k,i} = \langle H_{k,i} \rangle^2; \quad (2)$$

Here,  $k$  denotes the wave number of the Bloch state (MO) out of which the electron is removed and  $c_{k,i}$  ( $i = 1, 2, \dots$ ; see below for notation) are eigenstates of the ionized nanoring. We shall only consider ionization at zero temperature, that is, the nonionized system is initially prepared in its ground state. The quantities  $w_{k,i}$  are important, since the photoionization signals are proportional to them [22, 23, 24].

Symmetry considerations play an important part for ionization in nanorings, similar to optical absorption [13, 14]. In the latter case, the counterpart of the matrix elements in the r.h.s. of Eq. (2) entering the coefficient of optical absorption are the elements of the dipole operator  $\hat{P}$ . For the case of closed shells considered here, we have always found that the ground state possesses  $A_{1g}$  symmetry. In this case, because the dipole operator  $\hat{P}$  possesses  $E_{1u}$  symmetry [13, 14], only  $E_{1u}$  excited eigenstates can be targeted in optical absorption. To target eigenstates with symmetries different from  $E_{1u}$  by zero-temperature optical absorption, one needs to consider open shell rings, characterized by ground state symmetries  $\notin A_{1g}$ , as done in Ref. 14. The situation is different for ionization. The MOs span many irreducible representations  $\Gamma_k$  of the point group  $D_{Nh}$  [30]. Eigenstates  $\Gamma_{k,1}; \Gamma_{k,2}; \Gamma_{k,3}; \dots$  of all MO-symmetries (specified by the value of  $k$ ) can be targeted by ionization even with an initial neutral  $A_{1g}$  state (because  $\Gamma_k \otimes \Gamma_k = A_{1g}$ ). To this, it suffices to consider nanorings with closed shells. For the sake of simplicity, we shall restrict ourselves here to the prototypical case of closed shells, the half-filling case.

Numerical results will be presented for half-filled nanorings with six and ten QDs. For the former case, all eigenstates of Hamiltonian (1) can be computed exactly by numerical diagonalization: the dimension of the total Hilbert space is equal to 924 for the neutral ring and 792 for the ionized ring. The neutral ground state is a singlet, and one can carry out calculations in subspaces with total spin projection  $S_z = 0$  and  $S_z = \pm 1=2$ , respectively. The corresponding dimensions are then reduced to 400 and 300, respectively. The fact that all eigenstates of Hamiltonian (1) can be computed exactly enables us a very detailed analysis of all relevant physical aspects. For ten QD nanorings, the total dimension is equal to 184756 in neutral rings and 167960 in ionized rings. Similar to the above case, the restriction to the subspaces with  $S_z = 0$  and  $S_z = \pm 1=2$  is also possible, which results in the reduced dimensions of 63504 for neutral rings and 52920 for ionized rings. For such dimensions, the Lanczos algorithm has been applied. By running three times the Lanczos procedure we are able to compute the ionization energies and the spectroscopic factors individually [31]. The difference from calculations for optical absorption [13, 14, 32, 33] is that the first two Lanczos runs are carried out for the nonionized ring, while in the third run one must choose the normalized vector  $q_k; j_i$  as starting Lanczos vector separately for each symmetry  $\Gamma_k$  and perform calculations for the ionized ring.

It is worth noting at this point that the continued fraction algorithm, familiar in con-

densed matter physics [34, 35, 36], does not suffice for the present purpose, since it only allows calculations of convoluted spectra. The phenomenon of avoided crossing, often encountered in the study on optical absorption in QD nanorings [14] and also important for ionization (see Secs. IV A, IV B, and V), represents a typical situation where the information on convoluted spectra obtained by this algorithm is totally insufficient.

Especially for the case of larger nanorings, for which the Lanczos algorithm has to be applied, the following sum rule, straightforwardly deduced from Eq. (2),

$$\sum_i w_{k,i} = \langle \mathbf{J}_k^y, \mathbf{c}_k; j | \mathbf{J}_k^y | \mathbf{c}_k; j \rangle \quad (3)$$

turns out to be very useful as check of numerical calculations.

At the end of this section, we note that, similar to earlier works [13, 14], we safely rule out any spurious contribution, e. g., those of higher spin eigenstates. Because the ket state  $\mathbf{c}_{k,j} | j \rangle$  entering Eq. (2) is an exact eigenstate of both the total spin projection and the total spin,  $S_z = S = 1/2$  [37], only the spin doublet eigenstates  $\mathbf{c}_{k,i}$  can possess nonvanishing spectroscopic factors  $w_{k,i}$ . For the ionized six QD nanorings, out of the total 300 eigenstates with  $S_z = 1/2$  we only retained the 210 eigenstates with  $S_z = S = 1/2$ . In the calculations for the ionized ten QD nanorings, the starting Lanczos vector possesses the correct spin (see above), but accumulated numerical errors during the Lanczos iterations could yield Ritz vectors containing unphysical admixtures with other eigenstates. We can unambiguously exclude this possibility: we have stored all the relevant Ritz vectors (usually at most 100 vectors of dimensions 52920) and checked that they are very accurate eigenvectors with correct spin, and exhaust Eq. (3). Their dispersion was always found to be very small, comparable to that of the neutral eigenstate. In particular, it is at least 3–4 orders of magnitude smaller than the energy difference at avoiding crossings (see Sec. V).

### III. ELECTRON CORRELATIONS

The fact that electron correlations are very important for Ag QD nanorings was demonstrated in a series of previous works. Details can be found in Refs. 12, 13, 14, 15 and will be therefore largely omitted here. One can inspect, e. g., the MO occupancies; see Fig. 1b of Ref. 13 and Fig. 2 of Ref. 14 for ten QD nanorings. At half filling, up to say,  $d = 1.4$ , one can clearly distinguish lower, occupied MOs and upper, empty MOs, while towards  $d = 2$

practically all MOs are democratically occupied with half of the number of electrons they can accommodate. In the former case, electrons are completely delocalized over the whole nanoring, whereas in the latter, they are localized on QDs. Rephrasing in a more actual language, the quantum entanglement of electron states is nearly perfect in the limit of small interdot spacing ( $d \ll 1$ ), while electrons become practically disentangled for large interdot spacing ( $d \gg 2$ ). The curves for the von Neumann entropy  $S = -\text{Tr} \log \rho$  ( $\rho$  being the reduced density matrix) [47, 48], the quantity used to quantify quantum entanglement, presented in Fig. 1, nicely visualizes how the system smoothly evolves from the limit of perfect entanglement ( $S = 2$ ) to that of perfect disentanglement ( $S = 1$ ) by increasing  $d$ . For later purposes, it is also useful to monitor the weights  $p_0, p_1, p_2, \dots$  of the multielectronic configurations in the wave function where none or several QDs are doubly occupied ( $\sum_i p_i = 1$ ). The weights of these multielectronic configurations in the nonionized ground state are also shown in Fig. 1. Because electron hopping dominates at small  $d$ , one or even several QDs can be doubly occupied. On the contrary, on-site Coulomb repulsion  $U$  precludes double occupancy at larger  $d$ , where it is the dominant energy term, and all QDs tend to become singly occupied at half filling.

Within the MO approximation, Eq. (2) immediately yields  $w_{MO} = 1$  for all occupied electron Bloch states. Because Bloch states with  $+k$  and  $-k$  are degenerate for  $k \neq 0$ ;  $N=2$ , out of the  $N=2$  occupied Bloch states (for even  $N$ ) there should be one contribution from the state with  $k = 0$  and  $(N-2)=4$  contributions from the states with  $|k| \neq 0$ , i.e.,  $(N+2)=4$  distinct ionization signals within the MO. Therefore, to assess the validity of the single-particle picture, we shall (i) compare the number of spectral lines in the ionization spectrum with  $(N+2)=4$  and (ii) monitor the deviations from unity of the quantities  $w$ .

#### IV. RESULTS

In this section, we shall present in detail numerical results for ionization in half-filled nanorings consisting of six and ten QDs. Excepting for Fig. 4c, in all other cases of Secs. IV A and IV B we only depict the ionization signals with significant spectroscopic factors. In addition to these, there are numerous spectral lines of very small but still nonvanishing intensities, a fact to be discussed in Sec. V I.

Because of spatial symmetry, free (Bloch) electron states satisfy exactly the Hartree-Fock

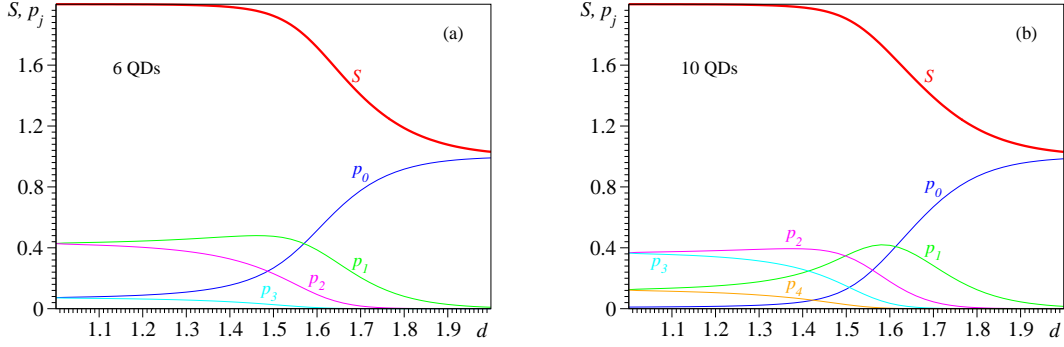


FIG. 1: (Color online) Dependence on the interdot spacing  $d$  of the entropy ( $S$ ) and the total weight  $p_0, p_1, p_2$  etc. of the multielectronic configurations in the neutral ground state of half-filled nanorings with no, one, two, etc. doubly occupied dots, respectively. For the nanoring with ten dots and electrons, the practically vanishing weight of the multielectronic configurations with five doubly occupied dots is not shown ( $p_5 \approx 0$ ). In both cases, for sufficiently distant QDs, the expansion of the neutral ground state is practically exhausted by multielectronic configurations for which none QD is doubly occupied ( $p_0 \approx 1$ ). The numbers of QDs in the nanoring are specified in the legend.

(SCF) equations (see e.g., Ref. 49). As a consequence, all ionization energies scale as the hopping integral  $t_0$  within the MO approximation. Therefore, the curves for MO ionization energies fall off exponentially with  $d$ . In the figures of this section, we shall not draw these rather trivial lines of the MO approximation. We shall present instead the less trivial curves (depicted by black dashed lines in the panels showing the ionization energies) for the lowest ionization energy  $\epsilon_{\text{loc}}$  in the large  $d$  limit, where electron hopping is negligible ( $t_0 \rightarrow 0$ ) and none QD is doubly occupied. In this limit, the energy of the neutral ground state is  $N \epsilon_{\text{H}} + N V$ . Removal of an electron from this state yields an ionized state with the energy  $(N-1)\epsilon_{\text{H}} + (N-2)V$ . The difference of these energies represents the lowest ionization energy  $\epsilon_{\text{loc}} = \epsilon_{\text{H}} - 2V$  in the limit of perfect localization.

Before going to discuss correlation effects on ionization spectra in detail, to give a flavor on the substantial difference between the MO and exact ionization spectra, we present an example in Fig. 2. Full spectra for all symmetries are shown in Fig. 2 for both six- and ten-dot nanorings, the two cases we shall later examine at length. There and in all of the other cases presented below, we have set  $\epsilon_{\text{H}} = -4.504 \text{ eV}$ , a choice that only fixes the



origin for energy [see Eq. (1)]. For a first glance assessment of the important role played by correlations for the spectra of Fig. 2 it suffices to say that, if the MO picture were valid, the spectra of Fig. 2a and 2b would only consist of two and three lines, respectively.

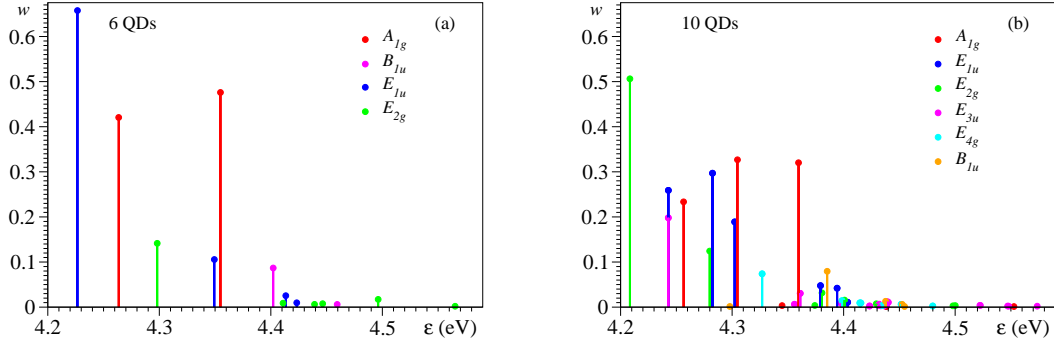


FIG. 2: (Color online) Exact ionization spectra for six and ten QD nanorings with interdot spacing  $d = 1.61$ . Notice that, in the MO spectra there exist only two and three lines (all with  $w = 1$ ), respectively. The MO lines are located at 4.556 eV and 4.609 eV in the former case, and at 4.536 eV, 4.589 eV, and 4.556 eV in the latter case.

#### A. Six-dot nanorings

Before discussing the numerical results for six-dot nanorings (point group  $D_{6h}$ ), it is useful to note that, within the single-particle picture, there are six MOs. Ordered by increasing energy these are: a nondegenerate  $a_{1g}$  MO ( $k = 0$ ), two degenerate  $e_{1u}$  ( $k = 1$ ) and  $e_g$  ( $k = 2$ ), and a nondegenerate  $b_{1u}$  MO ( $k = 3$ ). At half filling the  $a_{1g}$  and  $e_{1u}$  MOs are occupied by two and four electrons, respectively, whereas  $b_{1u}$  and  $e_{2g}$  MOs are empty.

From the multiplication table of the group  $D_{6h}$  and because the neutral ground state possesses  $A_{1g}$  symmetry, the ionization from an MO of a certain symmetry will bring the nanoring into a state of the same symmetry, e. g., removing an electron from an  $e_{1u}$  MO yields an ionized  $E_{1u}$ -state. Below, we shall discuss separately the ionization processes, depending on whether the MO wherefrom an electron is ejected would be occupied or not within the MO picture.

Within the MO picture only two ionization processes are possible, because only the  $a_{1g}$  and  $e_{1u}$  MOs are occupied. Accordingly, only two ionization processes (denoted by 1 in

Figs. 3a and 3c, respectively) are significant at small  $d$ . The latter, which corresponds to the lowest ionization energy (HOMO-ionization), brings the nanoring into the ionized ground state. It is denoted by 1 in Fig. 3c and was already considered in Ref. 12. With increasing  $d$ , the spectroscopic factors of these processes decrease from the MO {value  $w = 1$ . This represents one manifestation of electron correlations. Another manifestation is the fact that they become even significantly smaller than the corresponding MO occupancies:  $w_{k,1} < n_k$  ( $k = 0;1$ ). (Henceforth we omit the spin label whenever unnecessary and write, e. g.,  $n_k$  instead of  $n_{k,\uparrow}$ .) Compare the curves denoted by 1 with the MO populations  $n_0$ ,  $n_{A_{1g}}$  and  $n_1$ ,  $n_{E_{1u}}$  in Figs. 3a and 3c, respectively. According to the sum rule (3), other eigenstates should acquire significant spectroscopic factors, and this is indeed what one observes in Figs. 3a and 3c. The differences  $1 - n_{p,0}$  can be considered a measure of the extent to which electron correlations affect the  $e_u$  { and  $a_{1g}$  { MOs of the neutral ground state. In comparison with the  $A_{1g}$  { ionization spectrum, where two ionized  $A_{1g}$  { eigenstates practically exhaust all spectral weight in the whole  $d$ -range of interest, that for  $E_{1u}$  { symmetry is somewhat richer; compare Fig. 3a with Fig. 3c. In the latter case we encounter an avoided crossing at  $d = 1.633$ , where the energy difference between the curves denoted by 4 and 3 attains its minimum values of 28.7 meV. Later on in this paper we shall return to a more detailed analysis of the phenomenon of avoided crossing. Here we only note that, by considering the diabatic approximation for the states participating to this avoided crossing, basically only three (diabatic) states give nonvanishing contributions to the  $E_{1u}$  { spectrum.

Let us now switch to ionization from MOs that would be empty (in our case,  $e_{2g}$  and  $b_{1u}$ ) if the MO picture were valid. Such ionization processes are due to ground state correlations [24]; in the absence of the latter they do not obviously exist. Our results for these ionization processes are collected in Figs. 4 and 5. In accord with the fact that electron correlations in the neutral ground state increase with  $d$ , a general trend of increasing spectroscopic factors is visible in these figures. Particularly interesting is the  $E_{2g}$  { ionization spectrum, where a series of avoided crossings can be seen. As visible in Figs. 4a, one avoided crossing for each of the pairs of states (1, 2), (3, 4), and (5, 6) occurs at  $d' = 1.765$ ,  $d' = 1.685$ , and  $d' = 1.555$ , respectively. The corresponding minimum values of the energy differences amount 0.16 meV, 1.0 meV, and 3.1 meV, respectively. In fact, in the avoided crossing at  $d' = 1.555$ , not only two, but rather three (namely, 4, 5, and 6) states are involved. This fact is invisible in Fig. 4a, because the spectroscopic factor of the state 4 in this region is insignificant. In comparison

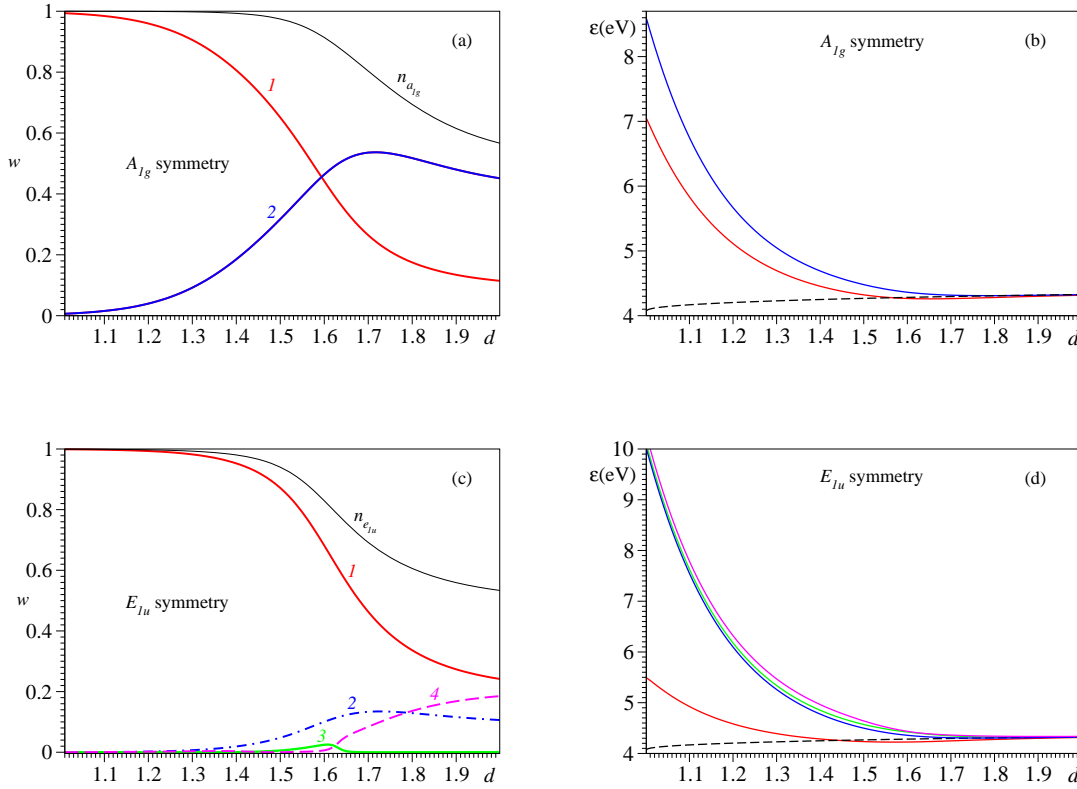


FIG. 3: (Color online)  $A_{1g}$  and  $E_{1u}$  spectral factors  $w$  and ionization energies  $\epsilon$  versus interdot spacing  $d$  in six-QD nanorings. The numbers  $i = 1, 2, \dots$  in the legend label the ionized eigenstates  $k, i$  [cf. Eq. (2)]. In panels (b) and (d), the black dashed line corresponds to the lowest ionization energy  $\epsilon_H = 2V$  in the limit of perfect localization.

with the  $E_{2g}$  spectrum, the spectroscopic factors of the  $B_{1u}$  spectrum are smaller: compare Fig. 5a with 4a. This agrees with the fact that the lower the unoccupied MO, the more it becomes populated due to the ground state correlations.

Actually, the states targeted by ionization in the case considered in this section represent eigenstates of a six-QD nanoring with five electrons. In this nanosystem, as discussed recently [14], optical absorption allows to target eigenstates of  $A_{1g}$ ,  $A_{2g}$  and  $E_{2g}$  symmetries. So, ionization and optical absorption provide complementary information. Some states can be studied only by one method ( $E_{1u}$  and  $B_{1u}$  states only by ionization,  $A_{2g}$  states only by optical absorption), while other states ( $A_{1g}$  and  $E_{2g}$ ) by both methods. For the latter, the information extracted from optical absorption can be compared with that from ionization. By comparing the ionization and optical absorption spectra for  $A_{1g}$ -symmetry (the present

Fig. 3a and Fig. 6f of Ref. 14, noting the logarithmic scale in the latter), one can conclude that, in both cases, only the first two  $A_{1g}$ -states give an important contribution. Likewise, the same first six  $E_{2g}$ -states are the only ones that are important both for ionization and for optical absorption: compare the present Fig. 4a with Fig. 6h of Ref. 14. Still, all the three avoiding crossings at  $d' = 1.765$ ,  $d' = 1.685$ , and  $d' = 1.555$  are visible in both spectra. The only difference is the participation in the optical absorption of three states at the avoided crossings at  $d' = 1.685$  and  $d' = 1.555$  (3, 4 and 5 in the former case, and 4, 5, and 6 in the latter), which is invisible in the  $E_{2g}$  ionization spectrum. This is due to the insignificant spectroscopic factors of the states 3 and 4 in the corresponding regions (see Fig. 4a).

## B. Ten-dot nanorings

For rings with ten QDs, within the single-particle picture there are ten MOs. Ordered by increasing energy, they are: a nondegenerate  $a_{1g}$  MO ( $k = 0$ ), two degenerate  $e_{1u}$  ( $k = 1$ ),  $e_{2g}$  ( $k = 2$ ),  $e_u$  ( $k = 3$ ),  $a_g$  ( $k = 4$ ) MOs, and a nondegenerate  $b_u$  MO ( $k = 5$ ). Similar to the case analyzed in Sec. IV A, the ejection of an electron from an MO of a given symmetry leads to a final ionized state of the same symmetry, e. g., removing an electron from an  $e_{4g}$  MO yields an ionized  $E_{4g}$  state. This follows from the properties of the  $D_{10h}$  point group and the fact that the neutral ground state possesses  $A_{1g}$  symmetry.

The numerical results for ionization in ten-dot nanorings are presented in Figs. 6 and 7, separately for each symmetry. They confirm the general features already observed in six-QD nanorings. For the ionization processes having the symmetries ( $A_{1g}$ ,  $E_{1u}$ , and  $E_{2g}$ ) of the MOs completely occupied within the MO picture (let us call them "occupied" MOs), there exist one signal (let us call it the "main" signal) per each symmetry whose spectroscopic factor is close to the ideal value  $w_{MO} = 1$  at  $d \ll 1$ . With increasing  $d$ , it decreases from  $w_{MO} = 1$  and becomes more and more smaller than the corresponding MO population ( $n_0 = n_{A_{1g}}$ ,  $n_1 = n_{E_{1u}}$ ,  $n_2 = n_{E_{2g}}$ ). Concomitantly, a few more ("satellite") signals acquire more and more significant spectral weight, such that at larger  $d$  they can even dominate over the "main" signal. See Fig. 6. Interestingly, the deeper the "occupied" MO, the more is it affected by correlations at larger  $d$ ; the relative weight of the "satellite" signals to the "main" signal for  $A_{1g}$  symmetry (deepest "occupied" MO) is larger than that for  $E_{1u}$  symmetry, which is in turn larger than for  $E_{2g}$  symmetry (highest "occupied" molecular

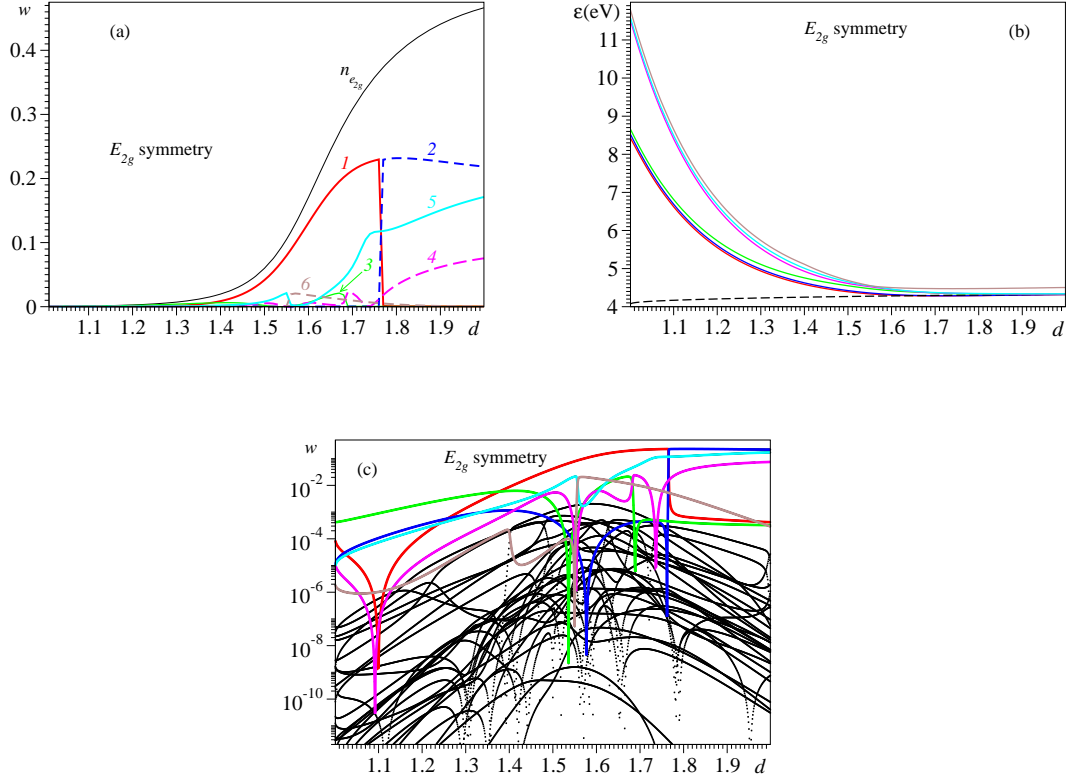


FIG. 4: (Color online)  $E_{2g}$  spectral factors  $w$  (a) and ionization energies  $\epsilon$  (b) versus interdot spacing  $d$  in six QD nanorings. The numbers  $i = 1, 2, \dots$  in the legend label the ionized eigenstates  $k_{\pm i}$  [cf. Eq. (2)]. In panel (b), the black dashed line corresponds to the lowest ionization energy  $\epsilon_H \approx 2V$  in the limit of perfect localization. Notice the numerous spectral lines with very small intensities in panel (c), which represents panel (a) redrawn using the logarithmic scale on the ordinate, demonstrating that the extended Hubbard model is characterized by a hidden quasi-symmetry (see Sec. VI).

orbital, HOMO).

At very small interdot distances ( $d \ll 1$ ), the ionization from the "unoccupied" MOs (i.e., those unoccupied if the MO picture were valid) is altogether ineffective. However, as a result of the strong electron correlations, the spectroscopic factors of these  $E_{3u}$ ,  $E_{4g}$ , and  $B_{1u}$  ionization processes gradually increase with increasing  $d$ . Their spectral weight also becomes distributed over several lines. Similar to that from the "occupied" MOs, these spectroscopic factors are comparable among themselves, and also with those of the relevant ionization signals of the "occupied" MOs. See Figs. 7 and compare them with Figs. 6.

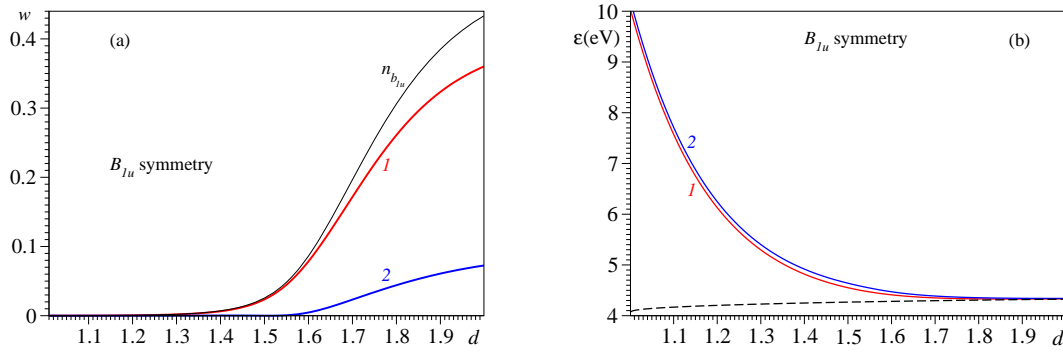


FIG. 5: (Color online)  $B_{1u}$  spectral factors  $w$  (a) and ionization energies  $\epsilon$  (b) versus interdot spacing  $d$  in six-QD nanorings. The numbers  $i = 1$  and  $2$  in the legend label the ionized eigenstates  $k_{ji}$  [cf. Eq. (2)]. In panel (b), the black dashed line corresponds to the lowest ionization energy  $\epsilon_H = 2$  V in the limit of perfect localization.

To conclude, similar to the case of six-dot nanorings of Sec. IV A, the MO picture rapidly deteriorates with increasing  $d$ .

From the inspection of the ionization factors of six-dot nanorings (Figs. 3, 4, and 5), one may be tempted to think that avoided crossings only occur for two-dimensional irreducible representations ( $E_{1u}$  and  $E_{2g}$  in that case) and not for the one-dimensional irreducible representations ( $A_{1g}$  and  $B_{1u}$ ). However, this is not true, as illustrated by the results for the one-dimensional irreducible representations of ten-dot nanorings presented in Figs. 6a and 7e. For  $A_{1g}$  symmetry, two avoided crossings are visible in Figs. 6a and b: one involving the states denoted by 3 and 4 at  $d' = 1.561$ , another with the participation of the states 4 and 5 at  $d' = 1.670$ . The corresponding minimum energy differences are  $5.33$  meV and  $0.26$  meV, respectively. As seen in Figs. 7e and f, the avoided crossings for  $B_{1u}$  symmetry are more numerous. One of them, that at  $d' = 1.643$ , even involves three states.

Similar to the case of six-dot nanorings (Sec. IV A), one can compare the information deduced by ionization for ionized nanorings with that obtained by optical absorption for nanorings with nine electrons and ten QDs. As discussed in Ref. 14, in the latter case one can target eigenstates of  $E_{1u}$  and  $E_{3u}$  symmetry.

Certain avoided crossings are visible both in ionization and in optical absorption spectra. This is the case for the avoided crossing at  $d' = 1.755$  involving the states 2 and 3, as well as the pretty broad one around  $d = 1.87$ . On the contrary, the dense avoided crossings

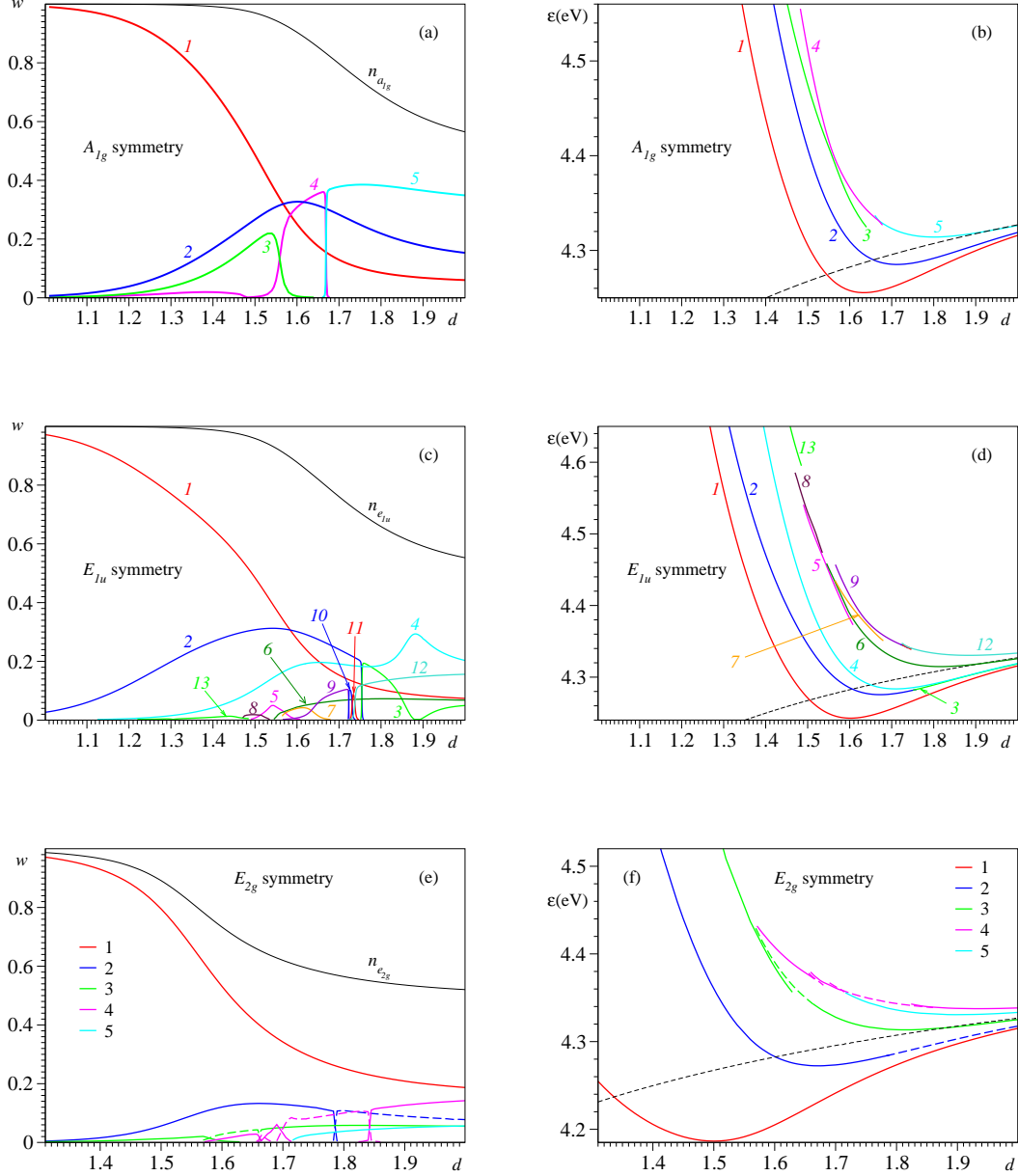


FIG. 6: (Color online)  $A_{1g}$ ,  $E_{1u}$ , and  $E_{2g}$  spectral factors  $w$  and ionization energies  $\epsilon$  versus interdot spacing  $d$  in ten QD nanorings. The numbers  $i = 1, 2, \dots$  in the legend label the ionized eigenstates  $\psi_{k,i}$  [cf. Eq. (2)]. In panel (d), the states 10 and 11 cannot be distinguished from the curves for 9 and 12 within the drawing accuracy. In panels (b), (d), and (f), the black dashed line corresponds to the lowest ionization energy  $\epsilon_H \approx 2V$  in the limit of perfect localization.

occurring in the narrow range  $1.723 \leq d \leq 1.737$ , which involve the states 9, 10, 11, and 12 can be seen only in ionization (Fig. 6c and d), but not in optical absorption, because of the

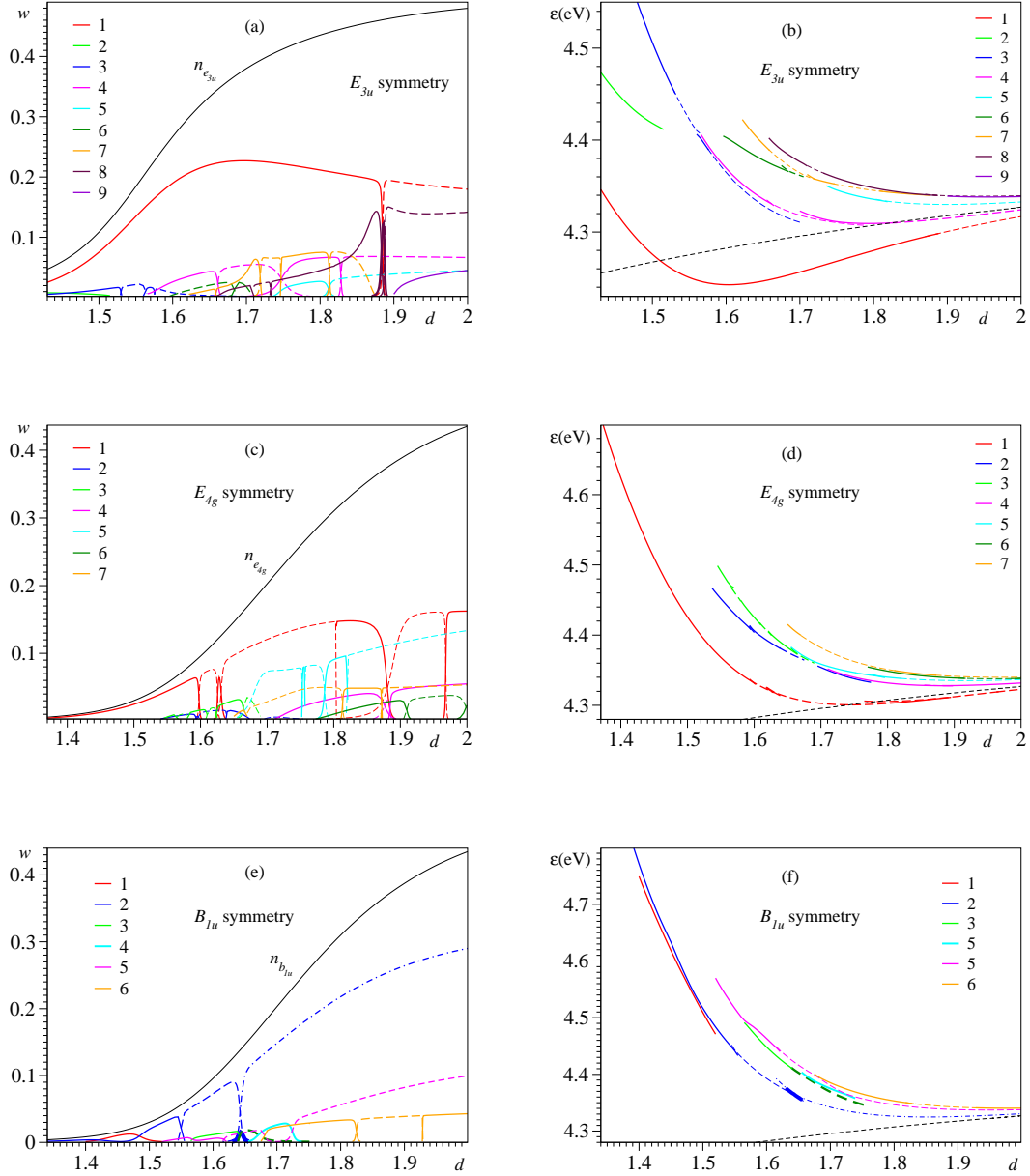


FIG. 7: (Color online)  $E_{3u}$ ,  $E_{4g}$ , and  $B_{1u}$  spectral factors  $w$  and ionization energies  $\epsilon$  versus interdot spacing  $d$  in ten QD nanorings. The numbers  $i = 1, 2, \dots$  in the legend label the ionized eigenstates  $\psi_{ki}$ . The black dashed line corresponds to the lowest ionization energy  $\epsilon_H \approx 2.0$  eV in the limit of perfect localization.

reduced intensities in the latter case; see Fig. 9d of Ref. 14.

The fact that more than two states can participate to an avoided crossing was already noted in the study on optical absorption [14]. An interesting situation can be seen in the



$E_{3u}$  spectrum (Fig. 7a and b), where two avoided crossings are visible around  $d' = 1.885$ : one at lower energies involves two states, another at higher energies with the participation of three states. These avoided crossings are insignificant for optical absorption, because of the reduced spectral intensity of these states [14].

A somewhat reversed situation occurs in the  $E_{3u}$  optical spectrum, where the participation of three states to the avoided crossing at  $d' = 1.525$  (see Fig. 9 of Ref. 14), while only two are significant (visible) in the  $E_{3u}$  ionization spectrum of Fig. 7a.

## V. AVOIDED CROSSINGS

The fact that avoided crossings involving energy curves of eigenstates of identical symmetries represent a frequent phenomenon in metallic QD nanorings has already been noted in the study of optical absorption [14]. As a general characterization, as visible in Figs. 4a, 6a, 6c, 6e, 7a, 7c, and 7e they only occur at larger  $d$ , where correlations are important. Two (or more) states of identical symmetry described by a single Slater determinant, where the MOs are either occupied or empty, cannot come too close in energy; basically, their energy difference is determined by the energy differences of their occupied MOs. Things change at larger  $d$ , where  $t_0$  ceases to be the dominant energy scale and frustration due to the  $U\{\}$  and  $V\{\}$  terms becomes important. For illustration, we present in Fig. 8 results for the pair of  $E_{2g}$ -states ( $E_{2g}^3$  and  $E_{2g}^4$ ) of the six-QD nanoring (cf. Fig. 4). As seen Fig. 8a, at the point  $d' = 1.685$  the weights of the multielectronic configurations where none, one, or two QDs are doubly occupied rapidly interchange between the mates involved in the avoided crossing. The contributions to energy of the  $t_0\{\}$ ,  $U\{\}$ , and  $V\{\}$  terms, i.e.,  $t_0^P = \sum_{k,j,i} h_{kji} j(a_{1i}^y a_{1+1i} + h.c.) j_{kji} i$ ,  $U^P = \sum_{k,j,i} h_{kji} j_{1i} n_{1i} j_{kji} i$ , and  $V^P = \sum_{k,j,i} h_{kji} j_{1i} n_{1+1i} j_{kji} i$ , respectively are sensitive to dot occupations. Indeed, their curves at the avoided crossing, depicted in Fig. 8b, behave accordingly.

One may ask at this point whether avoided crossings only occur in the extended Hubbard ring, or also in the restricted (i.e.,  $V = 0$ ) Hubbard ring. The results presented in Fig. 9, which represents the counterpart of Fig. 8 for  $V = 0$ , reveal that they are also present in the latter case. Again, the physics behind avoided crossings is the interplay between the competing terms (in this case  $t_0$ - and  $U$ -terms). For each eigenstate involved in an avoiding crossing, the individual ( $t_0\{\}$  and  $U\{\}$ ) terms exhibit jumps at the avoided crossing point that

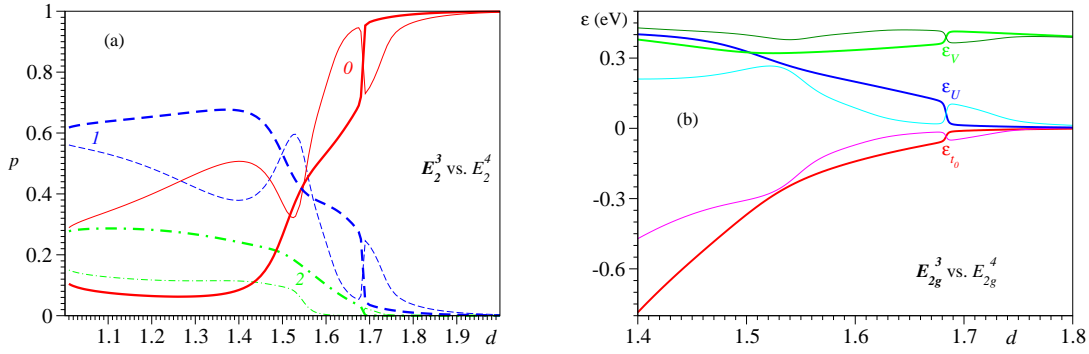


FIG. 8: (Color online)  $d$ -dependence of the weights  $p_0, p_1, p_2$  of the various multielectronic configurations (a) and the separate contributions of the  $t_0$ ,  $U$ , and  $V$  terms to the total energy (b) of the ionized eigenstates  $E_{2g}^3$  (thick lines) vs.  $E_{2g}^4$  (thin lines). See the main text and the caption of Fig. 1.

compensate each other in their sum (the total energy), which is represented by a smooth curve around this point. To avoid confusions, we note that the jumps at  $d \approx 1.495$  visible in Fig. 9 for the curves of the state  $E_{2g}^3$  are related to another avoided crossing between the states  $E_{2g}^3$  and  $E_{2g}^2$ . The latter, which is not shown in the figure, is characterized by jumps opposite to those for the  $E_{2g}^3$  curve.

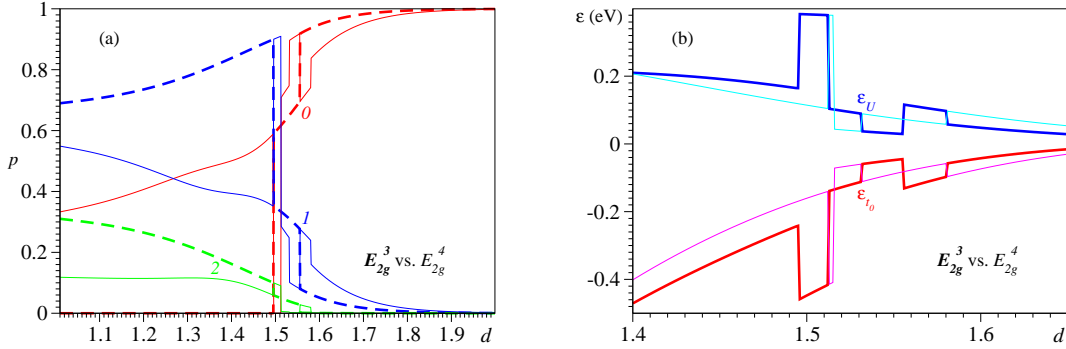


FIG. 9: (Color online)  $d$ -dependence of the weights  $p_0, p_1, p_2$  of the various multielectronic configurations (a) and separate contributions of  $t_0$  and  $V$  terms to the total energy (b) of the ionized eigenstates  $E_{2g}^3$  (thick lines) vs.  $E_{2g}^4$  (thin lines) in the case  $V = 0$ . See the main text and the caption of Fig. 1.

From a pragmatic standpoint, one may wonder whether avoided crossings are of impor-

tance at all; since what one can measure there is merely a smooth bright diabatic state, and not two (or several) individual (adiabatic) states with identical symmetry exhibiting rapid variations. However, one should mention that this applies to the case of the ideal nanoring with equidistant QDs. In a distorted nanoring, there will be avoided crossings between the ionization energies of the different symmetries of the ideal nanoring. Besides, similar to ordinary molecules [31], strong nonadiabatic effects can be expected in the presence of phonons.

## V I. H I D D E N Q U A S I { S Y M M E T R Y

Most importantly, this investigation gives further support to the most intriguing aspect of electron correlations previously encountered in optical absorption [14]: in spite of the fact that correlations are strong, out of very numerous ionized eigenstates allowed by spatial symmetry to contribute to the ionized spectrum, only very few states possess a significant spectroscopic factor.

The ionization spectra depicted in Figs. 2a and b are indeed richer than those, which comprise two and three lines, respectively, obtained within the MO approach. However, the number of the ionization signals is much smaller than the number of states, which are expected to contribute in a strongly correlated system. To properly assess the intriguing aspect of correlations, one should compare the number of significant ionization signals with the substantially larger number of states allowed to contribute by spatial symmetry and spin conservation. For the six-dot nanoring of Figs. 2a, there are ten significant ionization signals but 178 allowed transitions. For the ten-dot nanorings, the number of 15 lines visible in Figs. 2b should be compared with the number  $\sim 10^4$  of states allowed by spatial symmetry and spin conservation.

In addition to well established symmetries [38, 39, 40, 41, 42, 43, 44, 45], the restricted (i. e.,  $V = 0$ ) Hubbard model for rings is known to possess hidden symmetries [46]. Similar to the case of optical absorption, the scarcity of the ionized spectra of nanorings described by the extended Hubbard model discussed here points towards a hidden quasi-symmetry: besides a few signals with significant spectroscopic factors, there are numerous lines of very small but definitely non-vanishing intensities. These almost vanishing signals, which exhibit a regular dependence, can only be seen in Fig. 4c, due to the logarithmic scale on the

ordinate. In all of the other figures presented so far, they are invisible within the drawing accuracy. Therefore, one may be tempted to think that this hidden quasi-symmetry will evolve into a true hidden symmetry as  $V \rightarrow 0$ . However, this is not the case, and for illustration we present in Fig. 10 results for  $E_{2g}$  ionization in six QD nanorings for  $V = 0$ , which represents the counterpart of Fig. 4 at  $V \neq 0$ . The presence in Fig. 10c of numerous weak but non-vanishing spectral factors, also displaying a regular dependence and being many magnitude orders larger than inherent numerical inaccuracies, demonstrates that the restricted Hubbard model is also characterized by a hidden quasi-symmetry, similar to the extended Hubbard model.

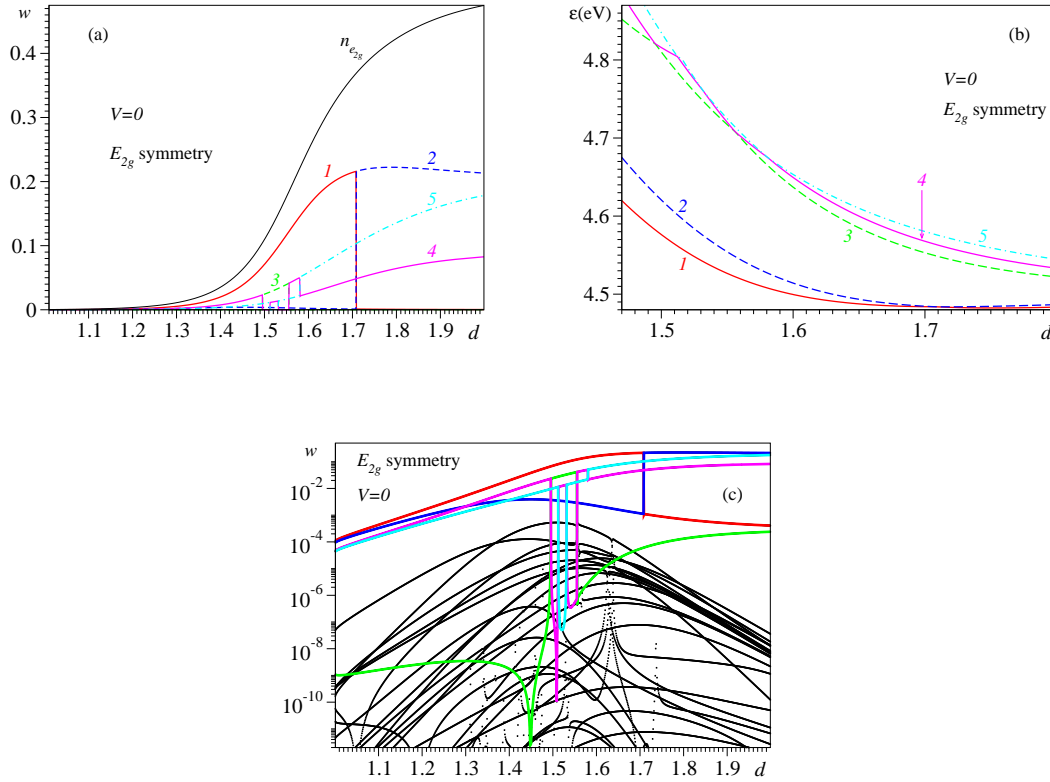


FIG. 10: (Color online)  $E_{2g}$  spectral factors  $w$  (a) and ionization energies  $\epsilon$  (b) versus interdot spacing  $d$  in six QD nanorings for  $V = 0$  (counterpart of Fig. 4). The numbers  $i = 1, 2, \dots$  in the legend label the ionized eigenstates  $|\kappa, i\rangle$  [cf. Eq. (2)]. Notice the numerous spectral lines with very small intensities in panel (c), which represents panel (a) redrawn using the logarithmic scale on the ordinate, demonstrating that the restricted Hubbard model is also characterized by a hidden quasi-symmetry.

Of course, the actual task of theory is to specify the hidden quasi-symmetry more precisely. An interesting observation concerns the number of significant spectral lines per each symmetry. As already noted, the number  $N_i$  of significant ionization signals is larger than expected within the MO picture, or, rephrasing, larger than the number  $N_{1h}$  of one-hole processes possible in the neutral self-consistent field (SCF)-ground state. However, this number can be comprehended if one considers in addition to  $N_{1h}$  the number  $N_{2h-1p}$  of two-hole-one-particle processes possible in the neutral SCF-ground state, wherein the excited electron occupies the MO just above the Fermi level. That is, the observation is that  $N_i = N_{1h} + N_{2h-1p}$ .

For instance, for a six-QD nanoring, there are two 1h-processes, one with  $A_{1g}$  and another with  $E_{1u}$  symmetry. The aforementioned 2h-1p-processes are represented by the products  $E_{1u}^1 E_{1u}^1 E_{2g}$ ,  $E_{1u}^1 A_{1g}^1 E_{2g}$ ,  $A_{1g}^1 E_{1u}^1 E_{2g}$ , and  $A_{1g}^1 A_{1g}^1 E_{2g}$ . By using the multiplication rules of  $D_{6h}$ , they lead to one  $A_{1g}$ , two  $E_{1u}$ , four  $E_{2g}$ , and two  $B_{1u}$ -processes. In this way, we arrive at two  $A_{1g}$ , three  $E_{1u}$ , four  $E_{2g}$ , and two  $B_{1u}$ -ionization processes. This is just what one observes in Figs. 3a, 3c, 4, and 5, respectively, if one considers the diabatic bright state at avoided crossings [50].

For ten-QD nanorings, there are three 1h-processes, of  $A_{1g}$ ,  $E_{1u}$ , and  $E_{2g}$  symmetry. The analysis is similar but more tedious for the relevant 2h-1p-processes. They are represented by the products  $E_{2g}^1 E_{2g}^1 E_{3u}$ ,  $E_{2g}^1 E_{1u}^1 E_{3u}$ ,  $E_{2g}^1 A_{1g}^1 E_{3u}$ ,  $E_{1u}^1 E_{2g}^1 E_{3u}$ ,  $E_{1u}^1 E_{1u}^1 E_{3u}$ ,  $E_{1u}^1 A_{1g}^1 E_{3u}$ ,  $A_{1g}^1 E_{2g}^1 E_{3u}$ ,  $A_{1g}^1 E_{1u}^1 E_{3u}$ , and  $A_{1g}^1 A_{1g}^1 E_{3u}$ . In view of the multiplication table of the point group  $D_{10h}$ , one gets three  $A_{1g}$ , five  $E_{1u}$ , five  $E_{2g}$ , six  $E_{3u}$ , six  $E_{4g}$ , and three  $B_{1u}$ -processes altogether. Again, these numbers agree with the numbers of significant ionization signals visible in Figs. 6 and 7, respectively.

The fact that for six-QD nanorings we can compute exactly all eigenstates enables us to continuously vary the model parameters and find out the counterparts of the states with significant spectroscopic factors in the limit  $d \rightarrow 1$ , where  $U, V \rightarrow 4t_0$  and the MO picture is reliable. The energies of the aforementioned 1h- and 2h-1p-processes are given in Table I for the limit  $U, V \rightarrow 0$ . For  $d \rightarrow 1$ , one finds  $t_0' = 1.49 \text{ eV}$ ,  $U = 4t_0' = 0.049$ , and  $V = 4t_0' = 0.036$ . By inspecting the curves for the ionization energies of Figs. 3b, 3d, 4, and 5 one can see that they compare favorably to those of Table I. In this limit, the main effect of interaction is to split the degenerate energies by amounts of the order of  $U$  and  $V$ . This demonstrates that, indeed, the ionization processes with significant spectroscopic factors evolve into the

TABLE I: The energies of the 1h{ and 2h-1p{processes described in the main text for six{QD nanorings in the limit  $U;V \rightarrow 0$ .

Symmetry	Process	Ionization Energy	Degeneracy
$E_{1u}$	1h	$\epsilon_H + t_0$	1
	2h-1p	$\epsilon_H + 4t_0$	2
$A_{1g}$	1h	$\epsilon_H + 2t_0$	1
	2h-1p	$\epsilon_H + 3t_0$	1
$E_{2g}$	2h-1p	$\epsilon_H + 3t_0$	3
	2h-1p	$\epsilon_H + 5t_0$	1
$B_{1u}$	2h-1p	$\epsilon_H + 4t_0$	2

1h{ and 2h-1p{processes occurring in the uncorrelated case.

For a quantitative description suggested by the above considerations, it appears most straightforwardly to employ  $c_{k,j,i}$  and  $c_{k,j,i}^y$  with  $k,j,k_1,j_1 = k_F$  and  $k_1,j_1 = k_F + 1$  for constructing linear independent vectors with appropriate spin and spatial symmetries. Here,  $k_F$  denotes the Fermi wave vector ( $k_F = n$  for closed shell rings with  $N = 4n + 2$ ,  $n$  being an integer) and  $j,i$  the exact neutral ground state [51]. We have used them as basis (sub)set for diagonalization, and found approximate eigenvectors  $\tilde{c}_{k,j,i}$  of the ionized nanoring. They have been utilized to compute an approximate ionization spectrum via Eq. (2). Apart from the fact that the number of lines is correctly obtained, this straightforward approach fails, however, to quantitatively reproduce the ionization spectra.

In the subsequent attempt to reproduce the ionization spectra, we have generalized this approach, by lifting the above constraints imposed on  $k,j,k_1$ , and  $k_2$ . In a further effort, we have alternatively employed the exact ionized ground state and the dressed particle{hole excitations  $c_{k_1,j_1,i}^y$  to construct a basis subset for diagonalization. Both aforementioned approximations are in the spirit of the treatment based on dressed particle-hole excitations developed in Ref. 14, where it turned out to be an insightful approximate method to study optical absorption. Unfortunately, none of these two methods is able to quantitatively reproduce the exact ionization spectra of strongly correlated QD {nanorings.

Similar to the case of optical absorption [13, 14], in spite of a variety of attempts of analyzing the numerical results, unfortunately, we cannot offer a quantitative explanation

of the hidden quasi-symmetry behind the scarcity of the ionization spectrum of strongly correlated nanorings. What we can do is only to tentatively speculate on the nature of this symmetry. Namely, based on the above considerations, we claim the existence of a one-to-one correspondence between the  $1h$  and  $2h-1p$  processes possible in the SCF (neutral ground state and the number of significant lines in the ionization spectrum of strongly correlated half-filled QD-nanorings described by the extended Hubbard model. The basic postulate of the Landau theory [52, 53, 54] is the one-to-one map between the low-energy excitations of noninteracting and interacting electron systems. Applied to ionization, Landau theory predicts a one-to-one correspondence between the ionization signals and the one-hole ( $1h$ ) ionized states, a fact contradicted by the exact ionization spectra. Therefore, our hypothesis on the number of relevant lines represents an extension of Landau's basic idea.

## V II. C O N C L U S I O N

Because of their widely tunable properties, metallic QDs assembled in regular nanoarrays represent ideal controllable systems for bridging the regimes of weak and strong correlations. The present study of ionization in metallic QD nanorings confirms the important impact of electron correlations found in a series of previous studies [12, 13, 14, 15]. It demonstrates that the MO-picture of ionization in tunable metallic QD-nanorings completely breaks down. This breakdown affects all MOs. In ordinary small molecules, it is possible to separate the ionization spectra of valence electrons in two distinct regions, related to outer- and inner-valence electrons [22, 23, 24]. In general, the MO-picture holds in the former but breaks down in the latter. Such a separation cannot be made in the metallic QD-nanorings investigated here, where strong correlations have impact on all of the MOs. As a limiting case thereof, even the HOMO ionization is drastically affected by correlations. This fact, already pointed out in Ref. 12, contrasts to the case of ordinary molecules. Nevertheless, there exists a similarity between QD-nanorings and ordinary molecules: as discussed in Sec. IV B, the higher "occupied" MOs are less affected by electron correlations than the lower ones.

In ordinary molecules, weaker electron correlations manifest themselves in ionization spectra as satellite lines of small intensities accompanying the main ionization signals [16, 17, 18, 19, 20, 21]. The main, more intense lines are the result of one-hole ( $1h$ ) processes related

to the ejection of an electron from an MO. The satellite, less intense lines are related to excitations accompanying the main ionization [55], often consisting of two-hole-one-particle (2h{1p) processes. In the case of strong correlations in molecules the intensity is distributed over numerous lines with comparable intensity. This effect was termed the breakdown of the molecular orbital picture of ionization [22, 23, 24]. Main lines cannot be identified in this case, because the properties of an ordinary molecule are not tunable, and tracing back to the uncorrelated limit is impossible.

The distinctive feature found in metallic QD-nanorings studied here is that, as visible in Figs. 3 and 6, in the presence of strong correlations the signals originating from the main lines of the uncorrelated case progressively lose intensity and become dominated by those that trace back to 2h{1p processes in uncorrelated nanorings. As concerns the number of lines in the ionization spectra, it remains astonishingly scarce. Along with the similar results of the recent studies on optical absorption [13, 14], this finding gives further support to the existence of a hidden quasi-symmetry in the metallic strongly correlated QD-nanorings described within the extended Hubbard model. As shown here, it remains a quasi-symmetry even in the case of the restricted Hubbard model ( $V = 0$ ).

With regards to the hidden quasi-symmetry, amply documented here and in other recent works [13, 14] by detailed numerical results, but for which a physical explanation is not yet available, we make the following remark. Exact numerical results played an important role in many cases, even including the Hubbard model. The fact that the one-dimensional restricted Hubbard model possesses accidental degeneracies was amply discussed in the literature in the past. What initiated this issue were the exact numerical results published long time ago for benzene-like rings [56]. Although a physical explanation could not be given that time, the finding on accidental degeneracies became part of wisdom for the Hubbard community. It was only much later that a demonstration that these "accidental" degeneracies follow from certain nontrivial conservation laws could be given [57]. Similarly, we hope that our numerical findings will stimulate further investigations to unravel the nature of the hidden quasi-symmetry put forward here.

We think that, the results of the present theoretical study on ionization along with those on optical absorption [13, 14] are of interest and hope that they will stimulate scientists to fabricate and investigate metallic QD-nanorings.



## Acknowledgements

The authors acknowledge with thanks the financial support provided by the Deutsche Forschungsgemeinschaft (DFG).

---

- [1] J. Heath, C. Knobler, and D. Le, *J. Phys. Chem. B* 101, 189 (1997).
- [2] C. P. Collier, R. J. Saykally, J. J. Shiang, S. E. Henrichs, and J. R. Heath, *Science* 277, 1978 (1997).
- [3] R. Ingram et al., *J. Amer. Chem. Soc.* 119, 9279 (1997).
- [4] G. M. Arkovich, C. P. Collier, and J. R. Heath, *Phys. Rev. Lett.* 80, 3807 (1998).
- [5] J. Shiang, J. Heath, C. Collier, and R. Saykally, *J. Phys. Chem. B* 102, 3425 (1998).
- [6] S. Chen et al., *Science* 280, 2098 (1998).
- [7] G. M. de Medeiros-Ribeiro, D. A. A. Ohlberg, R. S. Williams, and J. R. Heath, *Phys. Rev. B* 59, 1633 (1999).
- [8] S. Henrichs, C. Collier, R. Saykally, Y. Shen, and J. Heath, *J. Amer. Chem. Soc.* 122, 4077 (2000).
- [9] J. Sampaio, K. Beverly, and J. Heath, *J. Phys. Chem. B* 105, 8797 (2001).
- [10] K. Beverly, J. Sampaio, and J. Heath, *J. Phys. Chem. B* 106, 2131 (2002).
- [11] M. A. Kastner, *Physics Today* 46, 24 (1993).
- [12] I. Bâldea and L. S. Cederbaum, *Phys. Rev. Lett.* 89, 133003 (2002).
- [13] I. Bâldea and L. S. Cederbaum, *Phys. Rev. B* 75, 125323 (2007).
- [14] I. Bâldea and L. S. Cederbaum, *Phys. Rev. B* 77, 165339 (2008).
- [15] I. Bâldea, A. K. Gupta, L. S. Cederbaum, and N. Moiseyev, *Phys. Rev. B* 69, 245311 (2004).
- [16] K. Siegbahn et al., *ESCA - Atomic Molecular and Solid State Structures Studies by Means of Electron Spectroscopy*, North-Holland, Amsterdam, 1967.
- [17] K. Siegbahn et al., *ESCA - Applied to Free Molecules*, North-Holland, Amsterdam, 1969.
- [18] K. Siegbahn and L. Karlsson, in *Handbuch der Physik*, edited by S. Flugge, page 215, Springer, Heidelberg, 1982.
- [19] D. W. Turner, C. Baker, A. D. Baker, and C. R. Brundle, *Molecular Photoelectron Spectroscopy*, Wiley, New York, 1970.

- [20] J.W. Rabalais, Principles of Ultraviolet Photoelectron Spectroscopy, Wiley, New York, 1970.
- [21] J. Berkowitz, Photoabsorption, Photoionization and Photoelectron Spectroscopy, Academic Press, New York, 1979.
- [22] L.S. Cederbaum, J. Schirmer, W. Domcke, and W. von Niessen, J. Phys. B 10, L549 (1977).
- [23] L.S. Cederbaum, W. Domcke, J. Schirmer, and W. von Niessen, Physica Scripta 21, 481 (1980).
- [24] L.S. Cederbaum, W. Domcke, J. Schirmer, and W. von Niessen, Adv. Chem. Phys. 65, 115 (1986).
- [25] F. Remacle and R.D. Levine, J. Amer. Chem. Soc. 122, 4048 (2000).
- [26] F. Remacle et al., J. Phys. Chem. B 102, 7727 (1998).
- [27] F. Remacle, C.P. Collier, J.R. Heath, and R.D. Levine, Chem. Phys. Lett. 291, 453 (1998).
- [28] F. Remacle and R. Levine, J. Phys. Chem. B 105, 2153 (2001).
- [29] F. Remacle, K. Beverly, J. Heath, and R. Levine, J. Phys. Chem. B 106, 4116 (2002).
- [30] One should remark here that not all the symmetries of the group  $D_{Nh}$  are spanned by the MO-symmetries. This is the case, for example, of the eigenstates with  $A_{2g}$  or  $B_{2u}$  of a six-dot nanoring, which cannot therefore be studied by photoionization.
- [31] H. Koppel, W. Domcke, and L.S. Cederbaum, Adv. Chem. Phys. 57, 59 (1984).
- [32] I. Bâldea, H. Koppel, and L.S. Cederbaum, Phys. Rev. B 55, 1481 (1997).
- [33] I. Bâldea, H. Koppel, and L.S. Cederbaum, Phys. Rev. B 69, 075307 (2004).
- [34] D. Bulletin, R. Haydock, V. Heine, and M.J. Kelly, in Solid State Physics, edited by H. Ehrenreich, F. Seitz, and D. Turnbull, Academic, New York, 1980.
- [35] P. Fulde, Electron correlations in molecules and solids, in Springer Series in Solid-State Sciences, volume 100, Springer-Verlag (Berlin, Heidelberg, New York), 1991.
- [36] E. Dagotto, Rev. Mod. Phys. 66, 763 (1994).
- [37] The fact that  $\tilde{j}_{k,i} \propto \alpha_k$ ;  $j_i$  is a state of well defined  $S_z (= \pm 1/2)$  and  $S (= 1/2)$  straightforwardly follows from the commutation relations of  $\alpha_k$ , and the spin operators, and the fact that  $\hat{S}_z j_i = \hat{S}_+ j_i = 0$  ( $j_i$  is a singlet). The commutation relation  $[\hat{S}_z; \alpha_{k,\#}] = \frac{1}{2} \alpha_{k,\#}$  yields  $S_z \tilde{j}_{k,\#i} = +\frac{1}{2} \tilde{j}_{k,\#i}$ . Similarly, because  $\alpha_{k,\#}$  and the spin raising operator  $\hat{S}_+$  commute, one immediately gets  $S_+ \tilde{j}_{k,\#i} = 0$  and thence  $\hat{S}^2 \tilde{j}_{k,\#i} = (\hat{S}_z^2 + \hat{S}_- \hat{S}_+ + \hat{S}_z) \tilde{j}_{k,\#i} = \frac{3}{4} \tilde{j}_{k,\#i}$ .
- [38] A. Natan, Integrable models in condensed matter physics, in Series on Modern Condensed Matter Physics, Lecture Notes of ICTP Summer Course, edited by S. Lundquist, G. Morandi,

- and Y. Lu, volume 6, page 458, World Scientific Singapore, 1992.
- [39] A. Natan, Integrable models in condensed matter physics, 1994, cond-mat/9408101.
  - [40] E. H. Lieb and F. Y. Wu, Physica A: Statistical Mechanics and its Applications 321, 1 (2003).
  - [41] B. S. Shastry, Phys. Rev. Lett. 56, 1529 (1986).
  - [42] B. Shastry, J. Stat. Phys. 50, 57 (1988).
  - [43] H. Grosse, Lett. Math. Phys. 18, 151 (1989).
  - [44] M. Wadati, E. Omedilla, and Y. Akutsu, J. Phys. Soc. Jpn. 56, 1340 (1987).
  - [45] E. Omedilla and M. Wadati, Phys. Rev. Lett. 60, 1595 (1988).
  - [46] P. B. Ramos and M. J. Martins, J. Phys. A: Mathematical and General 30, L195 (1997).
  - [47] C. H. Bennett, H. J. Bernstein, S. Popescu, and B. Schumacher, Phys. Rev. A 53, 2046 (1996).
  - [48] G. C. Ghirardi and L. Marinatto, Phys. Rev. A 70, 012109 (2004).
  - [49] A. L. Fetter and J. D. Walecka, Quantum Theory of Many Particle Systems, McGraw Hill, New York, 1971.
  - [50] The bright diabatic state approximates the state with significant spectroscopic factor of a pair of states involved in an avoided crossing. For instance, in Fig. 4, it describes the state 1 for  $d < 1.765$  and the state 2 for  $d > 1.765$ .
  - [51] Unless  $d$  is very close to unity, using the SCF-ground state  $j_{SCF}$  instead of  $j_i$  is a very poor approximation, a fact easily understandable in view of the strong correlations.
  - [52] L. D. Landau, Sov. Phys. JETP 3, 920 (1956).
  - [53] L. D. Landau, Sov. Phys. JETP 5, 101 (1957).
  - [54] L. D. Landau, Sov. Phys. JETP 8, 70 (1959).
  - [55] T. Aberg, Phys. Rev. A 2, 1726 (1970).
  - [56] O. J. Heinmann and E. H. Lieb, Annals of the New York Academy of Sciences 172, 583 (1971).
  - [57] E. A. Yuzbashyan, B. L. Altshuler, and B. S. Shastry, J. Phys. A: Mathematical and General 35, 7525 (2002).